PHYSICS AND CHEMISTRY OF SOLID STATE
V. 24, No. 2 (2023) pp. 244-248
Section: Chemistry
DOI: 10.15330/pcss.24.2.244-248

Vasyl Stefanyk Precarpathian National University

ФІЗИКА І ХІМІЯ ТВЕРДОГО ТІЛА
Т. 24, № 2 (2023) С. 244-248
Хімічні науки

PACS: 75.75.Fk ISSN 1729-4428

Naresh Babu Gatchakayala, D. Rama Sekhara Reddy*

Synthesis, magnetic, ac conductivity and dielectric properties of hematite nanocrystallites

Department of Chemistry Krishna University, Machilipatnam 521004, Andhra Pradesh, India.dachuru@gmail.com

We are reporting the synthesis along with magnetic, ac conductivity and dielectric properties of hematite nanocrystallites. The prepared Fe_2O_3 is crystallizing in corundum structure which belongs to the rhombohedron system with the space group R3-c.The magnetization data shows a typical Morin transition, T_N = 265 K for 110 nm crystallites, whereas this transition is decreasing with decrease in crystallite size, T_N = 252 K for 33 nm. The value of magnetization is increased with increasing crystallite size. The enhanced dielectric permittivity and ac conductivity were observed in higher hematite crystallite size. The overall dielectric response has revealed conduction mechanism is due to the extrinsic contribution from the dominant Maxwell-Wagner polarization.

Keywords: hematite nanoparticles; Cole-Cole plot; Dielectric properties; Ac conductivity; Impedance.

Received 2 September2022; Accepted 10 March 2023.

Introduction

Recently, iron (Fe) and its oxides (Fe_3O_4 and Fe_2O_3) have attracted the field of research due to their potential applications [1-10]. The most stable known Fe state due to having lower Gibbs free energy and wide spread oxide phase of iron is *a*-Fe_2O_3. They have been employed in technology due to their non-toxicity and low cost as the members of catalysis, magnetic storage, anticorrosive agents and gas sensors. The crystal structure of *a*-Fe_2O_3 is rhombohedral or hexagonal with the space group R3c or D^6_{3d} [11]. The magnetic state of bulk *a*-Fe_2O_3 particles is "canted antiferromagnetic (weak ferromagnetism)" between 263 K and Neel temperature (~ 950 K) [12,13]. It is because of their unique structural property of hematite that the rhombohedral (1 1 1) planes form the layers of Fe^{3+} ions (T = 950 K to 260 K). These planes are separated by layers of oxygen (O^{2-}) ions. The spins of Fe^{3+} ions remained parallel in any (1 1 1) plane, i.e., ferromagnet, but adjacent planes are antiparallel, i.e., antiferromagnet. The canting between (1 1 1) plane produces uncompensated magnetic moments of Fe^{3+} spins between adjacent planes. Thus a weak ferromagnetism (or canted antiferromagnetism) is observed in hematite. The spin moments are completely turned perpendicular to the (1 1 1) plane below a typical temperature T_M ~ 260 K, known as Morin temperature, and *a*-Fe_2O_3 becomes a normal antiferromagnet [12,13]. This transition is a first order magnetic phase transition, which is dependent upon strain, particle size, crystallite, change at lattice parameters, and particle shape. Compared with bulk *a*-Fe_2O_3, the effects of lattice expansion, strain, defects, unpaired spins and broken symmetries have a grounded new magnetic behavior in nano sized *a*-Fe_2O_3. In this paper, we present the synthesis along with the magnetic, ac conductivity and dielectric properties of hematite nanocrystallites.

I. Experimental Details

Fe_2O_3 nanoparticles were synthesized by co-precipitation method. The metal nitrate $Fe(NO_3)_3$ 0.02 mole were added into 100 ml distilled water. A water solution of sodium hydroxide 50 ml with molarity 2 M were slowly added into the iron solution above. Precipitate is formed immediately. The precipitate was washed thoroughly with distilled water then filtered and dried at 80ºC for overnight. After drying, the hydroxed precipitate flakes were ground into powder. This

powder was segregated into different parts and heated for 3 h at different temperatures ranging from 550ºC to 1000ºC in air. The ramping rate was set 2ºC/min. and the cooling rate was 5ºC/min. After above procedure, the powders were pressed into pellets (10 mm diameter and 1~2 mm thickness) and annealed at the corresponding temperatures. These pellet samples were polished to produce a flat uniform surface and electrode with silver paint, then applied an AC voltage source for dielectric measurement.

II. Results and discussions

The *a*-Fe_2O_3 samples were prepared by co-precipitation method, and annealed in five different annealing temperatures T_A (550, 650, 750, 900, and 1000ºC). The obtained nanocrystallites are of Rhombohedral structure with space group *R3-c* [11]. X-ray diffraction pattern of the different annealing temperatures T_A (550, 650, 750, 900, and 1000ºC) samples are shown in Fig. 1 and no impurity being revealed. All the obtained samples are revealed Rhombohedral structure with space group *R3-c* [11]. The refined lattice constants are decreasing slightly from a = 5.028 Å, and c = 13.744 Å for T_A = 550ºC to a = 5.024 Å, c = 13.713 Å for T_A = 1000ºC as shown in Table I. The average crystallite sizes (determined from the XRD peak width employing the Scherrer relation) were found to be ~ 33 nm to ~ 110 nm with increasing annealing temperature from 550ºC to 1000ºC, which is indicated in Fig 1.

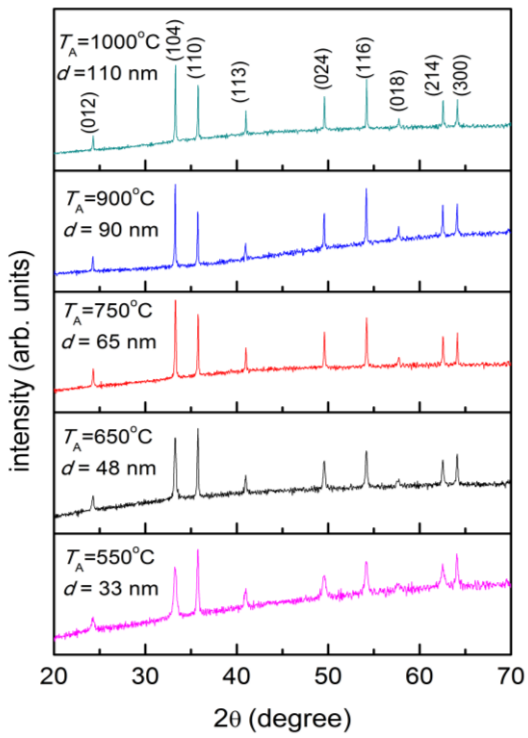

Fig. 1. X-ray diffraction pattern of the α-Fe_2O_3 nanocrystallites with different annealing temperatures and corresponding crystallite sizes.

Figure 2 shows the typical SEM micrographs for *a*-Fe_2O_3 particles prepared at different T_A's (a) 550ºC and (b) 1000ºC. The particle size and the morphology changes with T_A were observed. These microstructures were strongly influenced by T_A for all the particles.

The temperature dependence of magnetization of

Table 1.

The lattice constants of α-Fe_2O_3nanocrystallites

T_A = 550ºC d = 33 nm	T_A = 650 ºC d = 48 nm	T_A = 750 ºC d = 65 nm	T_A = 900 ºC d = 90 nm	T_A = 1000 ºC d = 110 nm
a = 5.028 Å b = 5.028 Å c = 13.744 Å V= 347.459 Å^3	a = 5.027 Å b = 5.027 Å c = 13.726 Å V= 346.866 Å^3	a = 5.027Å b = 5.027Å c = 13.721 Å V = 346.739 Å^3	a = 5.024 Å b = 5.024 Å c = 13.714 Å V = 346.149 Å^3	a = 5.024 Å b = 5.024 Å c = 13.713 Å V = 346.124 Å^3

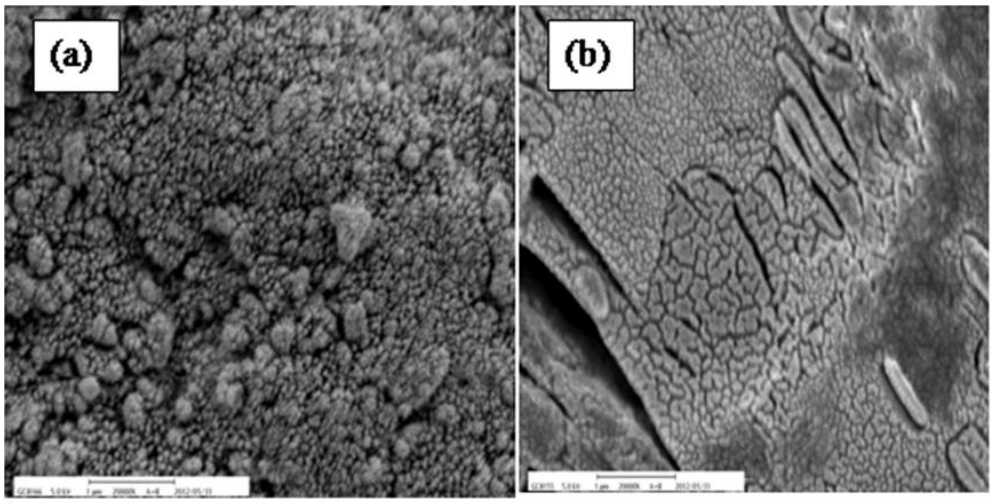

Fig. 2. SEM photos of theα-Fe_2O_3 samples of (a) 33 nm and (b) 110 nm.

a-Fe_2O_3 with different T_A's was depicted in Fig. 3. It revealed a magnetic transition around 265 K, named Morin transition for higher crystallites size of 110 nm (Figure 3a) whereas this transition is decreased with decrease in crystallites size for 33 nm particles the transition is at 252 K as shown in Fig. 3(b) [12,13]. Moreover, the magnetization value has increased with increase in crystallite size as observed in these nanocrystallites, which is related to quantum effects like surface effects.

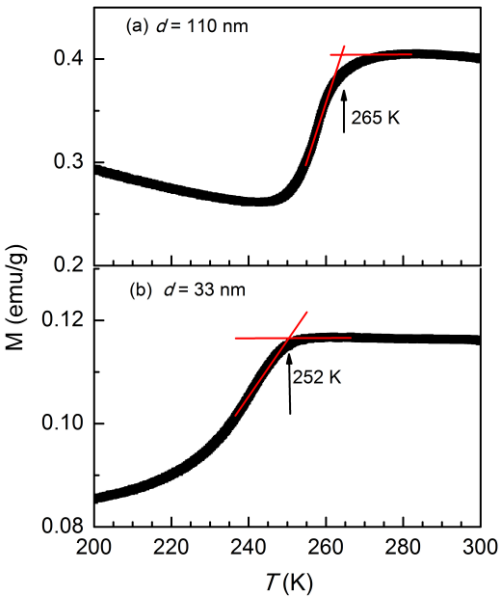

Fig. 3. Temperature dependent magnetization of α-Fe_2O_3(a) 110 nm and (b) 33 nm size crystallites.

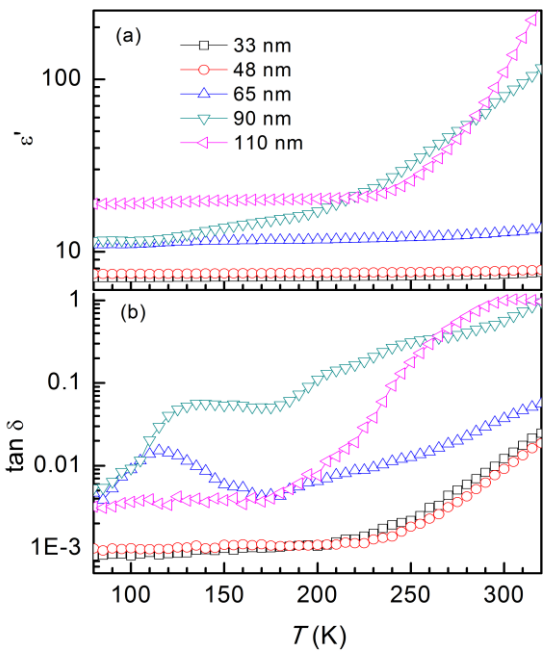

Fig. 4. ε'-*T* and tanδ-*T* relation of all nanocrsytallites of α-Fe_2O_3 at 1.5 kHz frequency.

Figure 4(a) shows the temperature dependent dielectric permittivity $\varepsilon'(T)$ at 1.5 kHz frequency for *a*-Fe_2O_3 with all crystallites sizes. $\varepsilon'(T)$ curves indicate that the ε' value increases with increasing crystallite size, which indicates the enhanced grain boundary. The imaginary part of dielectric loss tan$\delta(T)$ as a function of temperature at 1.5 kHz frequency for *a*-Fe_2O_3 with all crystallites sizes as depicted in Fig. 4(b).

Figure 5(a) shows the temperature dependent dielectric permittivity at different fixed frequencies for *a*- Fe_2O_3 with crystallites size of 33 nm. Below 250 K, $\varepsilon'(T)$ is independent of temperature and frequency, indicates intrinsic static dielectric constant value of $\varepsilon_S \sim 7.1$. Above 250 K, small increase in $\varepsilon'(T)$ is observed. Figure 4(b) shows the data of loss tangent (*tan*δ) as a function of temperature with selected test frequencies for 33 nm size crystallites of *a*-Fe_2O_3. The *tan*δ(*T*) curves also exhibit similar behavior like $\varepsilon'(T)$ curves and absence of peak below measured temperature range.

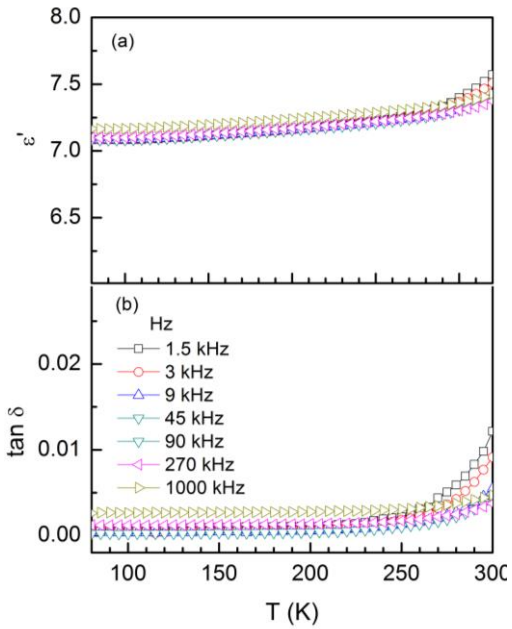

Fig. 5. ε''-*T* and tanδ-*T* relation of 33 nm nanocrystallites of *a*-Fe_2O_3.

Figure 6 shows the temperature dependent dielectric permittivity at different fixed frequencies for *a*-Fe_2O_3 with crystallite size of 110 nm. Below 250 K, $\varepsilon'(T)$ is independent of temperature and frequency and a small increase of intrinsic static dielectric constant value were observed of $\varepsilon_S \sim 19$. Above 250 K, small increase in $\varepsilon'(T)$ is observed. Figure 6 shows the data of loss tangent (*tan*δ) as a function of temperature with selected test frequencies for 110 nm size crystallites of *a*-Fe_2O_3. The *tan*δ(*T*) curves show a dielectric relaxation, where the step like increase in $\varepsilon'(T)$ curves. The relaxation is shifted to higher frequency with increasing temperature.

Increase in $\varepsilon^{/}$ of all samples rapidly with temperature at low frequencies could be either due to interfacial polarization or due to the accumulation of charged species at grain boundaries or dipolar polarizations which are strongly temperature dependent. The dispersion occurring in lower frequency regime may be attributed to interfacial polarization due to the charge accumulated at grain boundaries. The other reasons for dispersion may be due to space charge polarization, Maxwell Wagner, long range structural order and defect relaxations. The shifting of step

like dispersion to higher frequency region in the real part of the complex dielectric constant indicates that Maxwell Wagner relaxation mechanism was responsible for dispersive and large dielectric constant at low frequencies [14]. The dielectric behavior of such a material consists of a conducting or (semiconducting) grain separated by a more insulating grain boundary. The permittivity dispersion is insignificant at higher frequencies because atomic, electronic and molecular polarizations are responsible for high frequency permittivity which is independent of measured frequency range. The increase of ε' with the rise in temperature over the entire frequency range could be attributed related to the thermally activated process like charge carrier transportation.

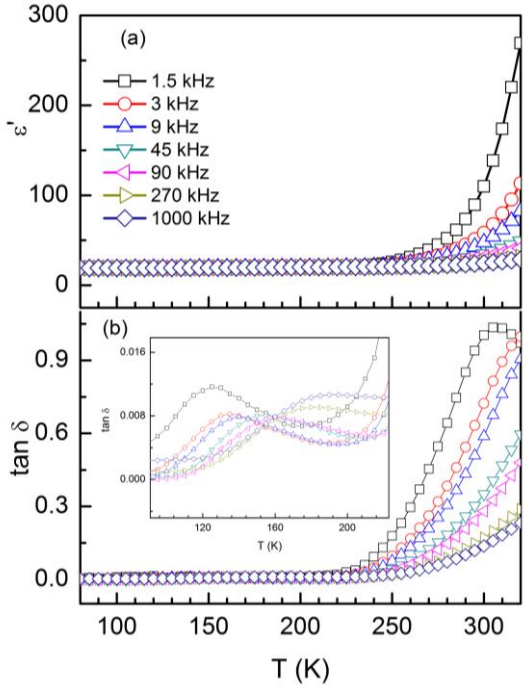

Fig. 6. ε'-T and tanδ-T relation of 110 nm nanocrystallites of α-Fe_2O_3.

The AC conductivity σ_{AC} as a function of test frequency *f* for different temperatures are shown in Figure 7 for *a*-Fe_2O_3 with crystallite size of (a) 33 nm and (b) 110 nm. The $\sigma_{AC}(f)$curves show different behavior in two ranges in all crystallite sizes. First, there is a strong rise at low frequencies. This is the grain-boundary blocking effect. Secondly, the conductivity does not increase as rapidly at high frequency. It is the bulk conductivity relaxation in which we are primarily interested. The σ_{AC} in the high frequency range can be described by "universal dielectric response" (UDR) [15]

$$\sigma_{AC} = \sigma_{DC} + \sigma_0 f^s \qquad (1)$$

Where σ_{DC} is the dc bulk conductivity, σ_0 is a constant, *f* is the rest frequency, and the exponent *s* is smaller than 1. Equation (1) is a common feature for all amorphous semiconductors and some other disordered systems. It is typical of thermal assisted tunneling between localized states.

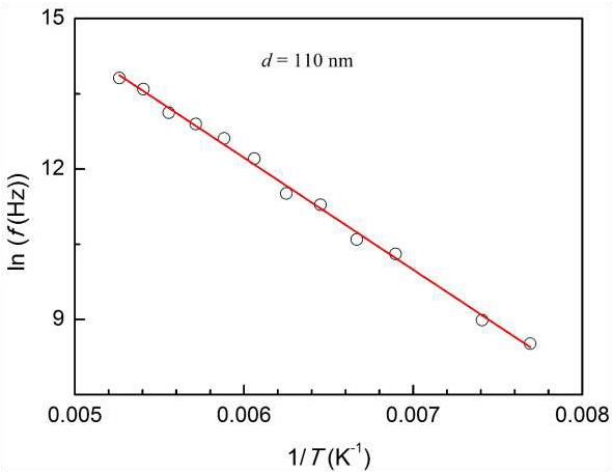

Fig. 7. Arrhenius plots for the observed relaxations of α-Fe_2O_3 of 110 nm size crystallites.

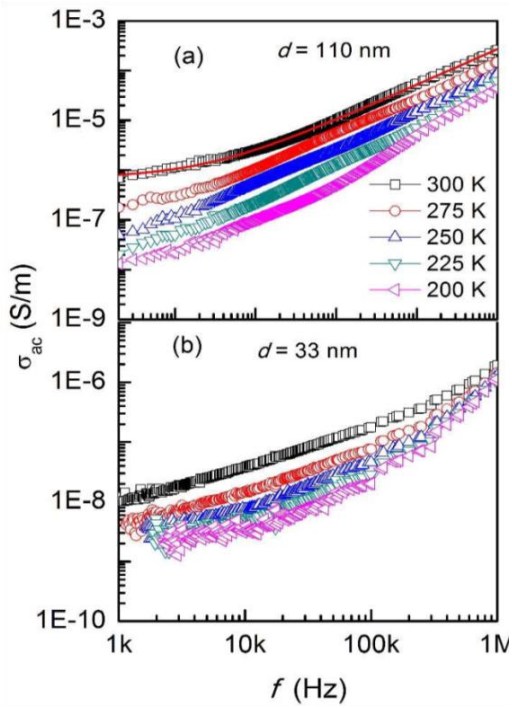

Fig. 8. Frequency dependent AC conductivity at fixed temperature of α-Fe_2O_3nanocrystallites (a) 110 nm and (b) 33 nm.

Conclusion

We report synthesis along with magnetic, ac conductivity and dielectric properties of hematite nanoparticles. As prepared Fe_2O_3 crystallizes in corundum structure which belongs to the rhombohedron system (space group *R3-c*). The magnetization data shows a typical Morin transition, T_N = 265 K for 110 nm crystallites, whereas this transition is decreasing with decreasing crystallite size, T_N = 252 K for 33 nm. The value of magnetization is increased with increasing crystallite size. The enhanced dielectric permittivity was observed in higher hematite crystallite size. The overall dielectric response has revealed conduction mechanism is due to the extrinsic contribution from the dominant Maxwell-Wagner polarization.

Acknowledgement

This research did not receive any specific grant from funding.

Declaration of competing interest

The authors declare that they have no known competing financial interests.

Naresh Babu Gatchakayala– Research Scholar of Krishna University;
D. Rama Sekhara Reddy– Asst.Professor at Krishna University.

[1] O.V. Salata, *Applications of nanoparticles in biology and medicine*, J. Nanobiotechnology, 2(1), 3 (2004); https://doi.org/10.1186/1477-3155-2-3.
[2] D.L. Huber, *Synthesis, properties, and applications of iron nanoparticles*, Small., 1(5), 482 (2005); https://doi.org/10.1002/smll.200500006.
[3] R.M. Cornell, U. Schwertmann, *The Iron Oxides: Structure, Properties, Reactions, Occurrences and Uses*. 2nd ed. John Wiley & Sons; (2006).
[4] S. Laurent, D. Forge, M. Port, et al. *Magnetic iron oxide nanoparticles: synthesis, stabilization, vectorization, physicochemical characterizations, and biological applications*, Chem Rev., 108(6), 2064 (2008); https://doi.org/10.1021/cr068445e.
[5] A.S. Teja,P-Y. Koh, *Synthesis, properties, and applications of magnetic iron oxide nanoparticles*, Prog Crystal Growth Char Mat., 55(1), 22(2009); http://dx.doi.org/10.1016/j.pcrysgrow.2008.08.003.
[6] M. De Cuyper, M. Joniau, *Magnetoliposomes*, Eur Biophys J., 15(5), 311 (1988);https://doi.org/10.1007/BF00256482.
[7] S. Hasany, I. Ahmed, J. Rajan, A. Rehman, *Systematic review of the preparation techniques of iron oxide magnetic nanoparticles*, Nanosci Nanotechnol, 2(6):148 (2012); https://doi.org/10.5923/j.nn.20120206.01.
[8] C-T. Wang, S-H. Ro, *Nanocluster iron oxide-silica aerogel catalysts for methanol partial oxidation*, Appl Catal A Gen., 285(1), 196 (2005); https://doi.org/10.1016/j.apcata.2005.02.029.
[9] A.K. Gupta, M. Gupta, *Synthesis and surface engineering of iron oxide nanoparticles for biomedical applications*, Biomaterials, 26(18), 3995(2005); https://doi.org/10.1016/j.biomaterials.2004.10.012.
[10] Attarad Ali, Hira Zafar, Muhammad Zia, Ihsan ul Haq, Abdul Rehman Phull, Joham Sarfraz Ali, Altaf Hussain, *Synthesis, characterization, applications, and challenges of iron oxide nanoparticles*, Nanotechnol Sci Appl. 9, 49 (2016); https://doi.org/10.2147/NSA.S99986.
[11] R.M. Cornell, U. Schwertmann, *Iron Oxides in the Laboratory: Preparation and Characterization*, 2nd ed.; Wiley-VCH: New York, NY, USA, 2000.
[12] J. G. Kim, K. H. Han, C. H. Lee and J. Y. Jeong, *Crystallographic and Magnetic Properties of Nanostructured Hematite Synthesized by the Sol-Gel Process*. J. Korean Phys. Soc., 38, 798 (2001);
[13] F. Bødker, M. F. Hansen, C. B. Koch, K. Lefmann and S. Mørup, *Magnetic properties of hematite nanoparticles*, Phys. Rev. B: Condens. Mater. Phys. 61, 6826 (2000); https://doi.org/10.1103/PhysRevB.61.6826.
[14] P. Lunkenheimer, V. Bobnar, A. V. Pronin, A. I. Ritus, A. A. Volkov, and A. Loidl, *Origin of apparent colossal dielectric constants*, Phys. Rev. B, 66, 052105 (2002); https://doi.org/10.1103/PhysRevB.66.052105.
[15] A. K. Jonscher, *Universal Relaxation Law*, (Chelsea Dielectrics Press, London, 1996).

Н.Б. Гатчакаяла,Р.С.Д. Дакуру

Синтез, магнітні, провідність змінного струму та діелектричні властивості та характеристики нанокристалітів гематиту

Хімічний факультет, Університету Крішни, Мачіліпатнам 521004, Андхра-Прадеш, Індія; dachuru@gmail.com

У статті наведено інформацію про синтез та магнітні властивості, провідність змінного струму, а також діелектричні властивості нанокристалітів гематиту. Отриманий Fe_2O_3 кристалізується в структурі корунду, що належить до системи ромбоедрів із просторовою групою *R3-c*. Дані намагніченості показують типовий перехід Моріна, T_N = 265 K для кристалітів 110 нм, тоді як цей перехід зменшується зі зменшенням розміру кристаліту, T_N = 252 K для 33 нм. Величина намагніченості збільшується зі збільшенням розміру кристалітів. Підвищені діелектрична проникність і провідність змінного струму спостерігалися у кристалів гематиту більших розмірів. Загальна діелектрична відповідь показала, що механізм провідності зумовлений зовнішнім внеском домінуючої поляризації Максвелла-Вагнера.

Ключові слова: нанокристали гематиту; точки Cole-Cole; діелектричні властивості; змінна провідність; імпеданс.